Carbohydrate Polymers 92 (2013) 167–175

Contents lists available at SciVerse ScienceDirect

Carbohydrate Polymers

journal homepage: www.elsevier.com/locate/carbpol

ZrO_2 surface chemically coated with hyaluronic acid hydrogel loading GDF-5 for osteogenesis in dentistry

Min Soo Bae[a,1], Ji Eun Kim[a,1], Jung Bok Lee[a], Dong Nyoung Heo[a], Dae Hyeok Yang[a], Jin-Ho Kim[b], Kung-Rock Kwon[b], Jae Beum Bang[c], Hojae Bae[a], Il Keun Kwon[a,*]

[a] Department of Maxillofacial Biomedical Engineering and Institute of Oral Biology, School of Dentistry, Kyung Hee University, 1 Hoegi-dong, Dongdaemun-gu, Seoul 130-701, Republic of Korea
[b] Department of Prosthodontics, School of Dentistry, Kyung Hee University, 1 Hoegi-dong, Dongdaemun-gu, Seoul 130-701, Republic of Korea
[c] Department of Dental Education, School of Dentistry, Kyung Hee University, 1 Hoegi-dong, Dongdaemun-gu, Seoul 130-701, Republic of Korea

ARTICLE INFO

Article history:
Received 20 June 2012
Received in revised form 28 August 2012
Accepted 24 September 2012
Available online 4 October 2012

Keywords:
Zirconium dioxide
Photo-cured hyaluronic acid hydrogel
Growth and differentiation factor-5
Bone morphogenetic protein-2
Release kinetics
Bone formation

ABSTRACT

The objective of this study was to modify zirconium dioxide (ZrO_2) with photo-cured hyaluronic acid hydrogel (pcHAgel), and to subsequently evaluate the bone regeneration potential of the modified ZrO_2. In the present study, HA grafted onto a ZrO_2 substrate was investigated for its biocompatibility and other properties. We describe the positive influences of ZrO_2 surface-modified with pcHAgel (Zr-3) containing two different loads of growth and differentiation factor-5 (GDF-5) to aid new bone formation as compared to the same amount of BMP-2 (Zr-4–7). We characterized the Zr-3 for their surface morphology and chemical properties. Atomic force microscopy (AFM), scanning electron microscope (SEM), and X-ray photoelectron spectroscopy (XPS) showed that the pcHAgel was successfully grafted onto the ZrO_2 surface. The sustained release of GDF-5 and BMP-2 were observed to occur in the Zr-4–7. *In vitro* cell tests showed a higher level of MG63 cell proliferation and differentiation on Zr-4–7 than on Zr-3. The Zr-3 is a good biomaterial to deliver osteogenic differentiation factors such as BMP-2 and GDF-5, and GDF-5 can be useful as an effective alternative to aid new bone formation as compared to BMP-2.

1. Introduction

Osseointegration is one of the most important criteria for the success or failure of bone anchored metallic implants in dentistry (Brånemark, Brånemark, Rydevik, & Myers, 2001). One of the most critical challenges to osseointegration is successfully anchoring metallic implants through stable attachment to alveolar bone. Successfully anchored metallic implants undergo a process which homogeneously combines with alveolar bone by directly depositing new bone onto their surfaces through favorable interactions with osteoblasts (Webster, Ergun, Doremus, Siegel, & Bizios, 2000).

Over the last several decades, titanium (Ti) and its alloys have been introduced as suitable materials for tooth reconstruction due to their chemical stability, mechanical strength, and excellent biocompatibility (Pourbaix, 1984). However, despite these functional merits, there has been a steady growing demand in the market for enhanced aesthetic features as well.

Zirconium dioxide (ZrO_2) is replacing Ti as a material for dental implants due to its aesthetic quality as it appears very similar to original teeth as well as having good chemical resistance, mechanical strength, and excellent biocompatibility (Chevalier, 2006). It has a flexural strength of ~900 MPa, a fracture toughness of up to 10 MPa/$m^{0.5}$, and an elastic modulus of ~210 GPa, which are superior mechanical properties than that of Ti (Garvie, Hannink, & Pascoe, 1975; Piconi et al., 1998). To improve the performance of Zr, its surface has been modified by using various methodologies, including ultraviolet (UV) light treatment, for enhanced bone integration (Att et al., 2009).

Recently, incorporation of a thin hydrogel layer on metallic solid surfaces has been reported to provide several advantageous functions for biomedical applications including micro-patterning and controlled drug release (Choi, Konno, Matsuno, Takai, & Ishihara, 2008; Sidorenko, Krupenkin, Taylor, Fratzl, & Aizenberg, 2007; Tokarev & Minko, 2010). For example, Ishihara's group reported that a surface-treatment method using 2-methacryloyloxyethyl phosphorylcholine (MPC) and a photo-labile linker could selectively regulate the attachment of MC-3T3 E1 cells on a glass surface (Choi et al., 2008). They also reported that a multilayered phospholipid polymer, synthesized with MPC, *n*-butyl methacrylate (BMA), and 4-vinylphenylboronic acid units (VPBC), coated on a titanium alloy surface could control the release of a hydrophobic antineoplastic agent, paclitaxel (PTX). This technique can be applied to provide localized drug delivery from metal-based biomedical

* Corresponding author. Tel.: +82 2 961 0350.
E-mail address: kwoni@khu.ac.kr (I.K. Kwon).
[1] Two first authors equally contributed to this work.

0144-8617/$ – see front matter © 2012 Elsevier Ltd. All rights reserved.
http://dx.doi.org/10.1016/j.carbpol.2012.09.044

devices (Choi et al., 2008). Hydrogel formation on a metallic solid surface has been fabricated by several methodologies, including layer-by-layer (LBL) self-assembly, photopolymerization, and radical polymerization (Choi et al., 2008; Yakushiji et al., 1999). Photopolymerization is one of the most adaptable methods for hydrogel coating on metallic solid surfaces by providing control over temporal and spatial reaction kinetics (Clapper, Sievens-Figueroa, & Guymon, 2008; Hiemstra, Zhou, Zhong, Wouters, & Feijen, 2007; Hutchison, Stark, Hawker, & Anseth, 2005). Moreover, photopolymerization can be achieved in a single, rapid-step process (Clapper et al., 2008; Hiemstra et al., 2007; Hutchison et al., 2005).

Hyaluronic acid (HA), a linear D-glucuronic acid and N-acetyl-D-glucosamine copolymer, has been known as a good macromolecule for many biomedical applications due to its hydrodynamic characteristics, viscous properties, and excellent water uptake (Gerecht et al., 2007; Kogan, Soltés, Stern, & Gemeiner, 2007). It has good hydrophilicity due to negatively-charged functional groups (Kogan et al., 2007).

Recent attention has been drawn to growth and differentiation factor-5 (GDF-5), another member of the BMP family (Hötten et al., 1996). The GDF-5 has been recognized as an important factor in limb development (Buxton, Edwards, Archer, & Francis-West, 2001; Hötten et al., 1996). The GDF-5 has also been expressed in bovine and rat tooth germs in cells associated with periodontal ligament (PDL) formation and cells located along the alveolar bone and cementum surfaces during the course of root formation, suggesting that GDF-5 may play regulatory roles in the development of the periodontal attachment (Morotome, Goseki-Sone, Ishikawa, & Oida, 1998; Sena et al., 2003). Recent *in vivo* studies with the addition of rhGDF-5 have reported significantly enhanced alveolar bone and cementum formation in a canine intra-bony defect model (Lee et al., 2010), as well as bone formation in both pre-clinical and clinical sinus augmentation studies (Gruber et al., 2009; Koch, Becker, Terheyden, Capsius, & Wagner, 2010). GDF-5 also interacts with limb-building BMP (Brunet, McMahon, McMahon, & Harland, 1998) and is more cost effective than osteogenic bone morphogenetic protein-2 (BMP-2) (Kim et al., 2011).

In this study, we designed and prepared surface functionalized ZrO_2 modified with photo-cured HA hydrogels containing two different amounts of BMP-2 and GDF-5 (10 and 50 ng) (**ZrO_2-4–7**) (Fig. 1), and evaluated their influence on new bone formation. To our knowledge, little is known about the surface modification technique of ZrO_2 with hydrogel containing osteogenic differentiation factors.

2. Materials and methods

2.1. Materials

Hyaluronic acid (HA) (Mw: 1700 kDa) was purchased from Lifecore Biomedical Co. (Chaska, MN, USA). Zirconium dioxide (ZrO_2) disks (diameter: 1 cm) were kindly obtained from DIO Co. (Busan, Republic of Korea). 2-Morpholinoethanesulfonic acid (MES), 2-aminoethylmethacrylate (AEMA), dexamethasone, alkaline phosphatase (ALP) assay kit, ascorbic acid, cetylpyridinium chloride and β-glycerophosphate were purchased from Sigma–Aldrich, Inc. (St. Louis, MO, USA). A cytocompatible photoinitiator, 4-(2-hydroxy ethoxy)phenyl-(2-hydroxy-2-propyl)ketone (Irgacure D-2959), was purchased from Ciba Geigy Ltd. (Basle, Switzerland). 1-Ethyl-3-(3-dimethyaminopropyl)-carbodiimide (EDC), and N-hydroxysuccinimide (NHS) were purchased from Tokyo Chemical Industry CO., Ltd. (TCI, Japan). Growth and differentiation factor-5 (GDF-5) was purchased from Preprotect Inc. (Rocky Hill, NJ, USA). Bone morphogenetic protein-2 (BMP-2) was purchased from R&D Systems (Minneapolis, MN, USA). Fetal bovine serum (FBS), penicillin/streptomycin, high-glucose Dulbecco's Modified Eagle's Medium (DMEM) and trypsin were purchased from GIBCO BRL (Carlsbad, CA, USA). Human osteosarcoma cell line (MG-63) cells and RAW 264.7 (mouse macrophage) cells were purchased from the Korean Cell Bank (Seoul, Republic of Korea).

2.2. ZrO_2 surface-modified with photo-cured HA hydrogels (*pcHAgel*) containing two amounts (10 and 50 ng) of BMP-2 and GDF-5 (**ZrO_2-4–7**)

The functionalized **ZrO_2-4–7** were engineered according to three procedures (Fig. 1). In the first procedure, a concentrated aqueous NaOH solution (2.5 M) was added to pristine **ZrO_2-1** and heated to 60 °C for 24 h in order to form active OH groups on the surface (**ZrO_2-1′**) (Uchida, Kim, Miyaji, Kokubo, & Nakamura, 2002). After washing with distilled water several times, the activated **ZrO_2-1′** was mixed in anhydrous toluene. To this mixture 2-aminopropyltriethoxysilane (APTES) (5 mL, 5% (v/v) solution) was added, and then reacted at 120 °C for 24 h. This reaction formed APTES-conjugated ZrO_2 (**ZrO_2-2**) (Fig. 1A). For the second procedure, 2-aminoethyl methacrylate (AEMA)-conjugated HA (**HA-AEMA**) was synthesized according to our previous report (Bae et al., 2011). Briefly, HA (1 g) was dissolved in MES buffer solution (50 mM, pH 6.5), and then NHS (1.06 g, 0.09 mol) and EDC (3.50 g, 0.22 mol) were added to the reaction solution. After stirring for 1 h, AEMA (400 mg) was added, and then continuously stirred at room temperature for 24 h. After dialysis (MWCO: 3500) against distilled water for 3 days, the aqueous solution of functionalized **HA-AEMA** was filtered, evaporated and lyophilized with blocking penetration of light (Fig. 1B). The reaction was confirmed by ^{1}H NMR (Varian Unity Plus 300, Varian Inc., Palo Alto, CA, USA) spectrometer (300 MHz) and ATR-FTIR (TENSOR 37, Bruker, USA) as reported previously (Bae et al., 2011). After dissolving **HA-AEMA** (1 g) in MES buffer solution (10 mL, pH 6.5), the solution was chemical conjugated to **ZrO_2-2** using NHS (0.11 g, 0.09 mol) and EDC (0.35 g, 0.22 mol). The reaction was carried out at room temperature for 24 h in order to conjugate **HA-AEMA** onto **ZrO_2-2** through amide bonds (**ZrO_2-3**). After washing with distilled water several times, a mixture of 0.05% (w/v) cytocompatible photoinitiator Irgacure D-2959 in distilled water (10 μL), two amounts of functional factor BMP-2 and GDF-5 (10 and 50 ng) were added, respectively. Following this each of the mixture put onto **ZrO_2-3** was exposed to UV light (CL-1000 UV-crosslinker, 365 nm, UVP) (Jeon, Bouhadir, Mansour, & Alsberg, 2009) at room temperature for 5 min. This formed the photo-cured HA hydrogel film on **ZrO_2-3** containing either BMP-2 or GDF-5 (**ZrO_2-4–7**) as depicted in Fig. 1C.

2.3. Surface characterization of ***ZrO_2-1***, ***2***, and ***3′***

Scanning electron microscopy (SEM, S-2300, Hitachi, Japan) observations were carried out on dried **ZrO_2-1**, **2** and **3′**gold-coated by using a sputter-coater (Eiko IB, Japan) under an accelerating voltage of 15 kV. X-ray photoelectron spectroscopy (XPS) measurements were carried out with a Thermo Electron (U.K.) at a grazing angle of 90° under high vacuum ($<3.1 \times 10^{-9}$ Torr). A monochromatic aluminum Kα X-ray radiation (photoelectron energy = 1486.6 eV) was used and the wide-scanned XPS spectra was obtained at a pass energy of 187.8 eV. Static contact angle measurements using a sessile drop method was carried out on three Zr specimens at 20 °C with 3 μL of distilled water droplet under a relative humidity of 60%, in advance ajusted to 71.8 mN/m of surface tension, as measured by a telescopic goniometer (Pheonix 300, SEO, Republic of Korea). Tapping mode atomic force microscopy (TM-AFM) observations were carried out in wet condition by using a NANOS® TM-AFM system (NanoInk, Inc., USA). The

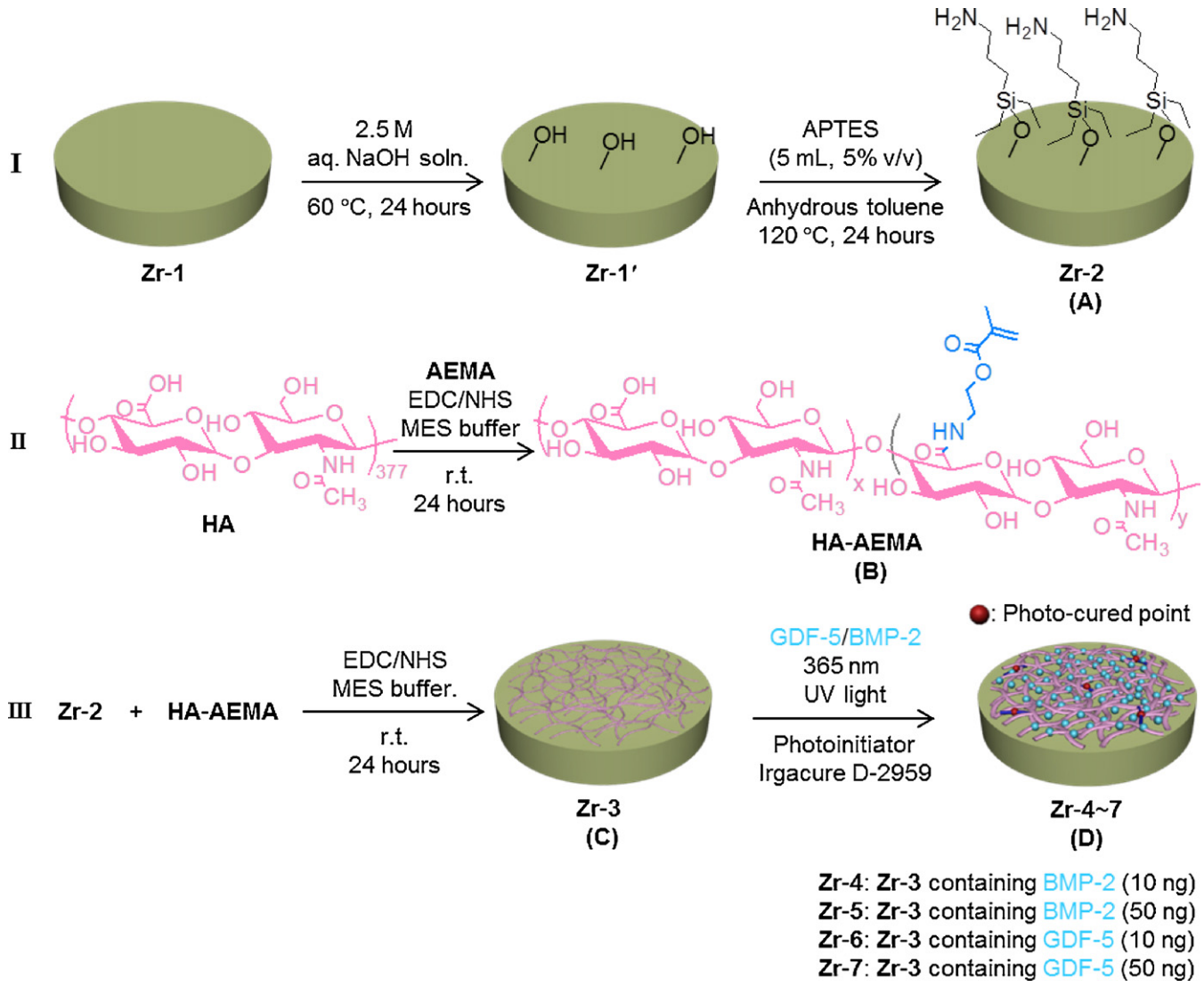

Fig. 1. Schematic illustration for the preparation of **Zr-4–7**. The **Zr-4–7** was prepared by four steps as follows: (A) preparations of **Zr-2**, (B) **HA-AEMA**, (C) the conjugation of **HA-AEMA** on the surface of **Zr-2** *via* amid bonds and (D) preparation of **Zr-4–7**.

TM-AFM observation was measured at an ambient temperature under a 1.5 Hz scan rate. Digital TM-AFM images were acquired by using SPIPTM program (Scanning Probe Image Processor, Probes, Republic of Korea).

2.4. Protein adsorption assay of ZrO_2-1, 2, and 3′

The adsorption of protein was evaluated by using bovine serum albumin (BSA, St. Louis, MO, USA). **ZrO_2-1**, **2** and **3′** were dipped into 500 μL of BSA (1 mg/mL, PBS (pH 7.4)). After 6 and 24 h of incubation at 37 °C, the non-adsorbed BSA was rinsed with PBS (pH 7.4) solution several times. After this, Bradford solution (Bio-Rad, Hercules, CA, USA) was added to **ZrO_2-1**, **2** and **3′** surfaces at 37 °C for 1 h. The BSA concentration was determined by using a Bradford assay according to the manufacturer's instructions. The absorbance was measured by using a microplate reader (Bio-Rad, Hercules, CA, USA) at a wavelength of 595 nm.

2.5. Release kinetics of BMP-2 and GDF-5 from ZrO_2-4–7

ZrO_2-4–7 were each immersed in centrifuge tubes containing 1 mL of PBS (pH 7.4) solution, and then incubated at 37 °C with a continuous agitation at 50 rpm. At predetermined time points of 1, 3, 6, 24 h, 3, 7, 14, 21 and 28 days, each supernatant was extracted from the centrifuge tubes and assayed by using two kinds of ELISA kits (BMP-2 kit: Quantikine, R&D system, Minneapolis, MN, USA and GDF-5 kit Uscn Life Science Inc., Wuhan, China) to confirm sustained release as well as existence of BMP-2 and GDF-5. The absorption of each sample was read at 495 nm using a microplate reader. The amounts of BMP-2 and GDF-5 were calculated by using a calibration curve based on a series of known standard concentrations of BMP-2 and GDF-5, respectively. This experiment was carried out in triplicate.

2.6. Inflammatory test of ZrO_2-1, 2 and 3′, 5 and 7

RAW 264.7 (mouse macrophage) cells were obtained from the Korean Cell Lines Bank (KCLB) and were cultured in minimum essential medium (MEM) alpha (GIBCO, NY, USA) supplemented with 10% of FBS (GIBCO, NY, USA) and 1% of antibiotic–antimycotic in a humidified 5% of CO_2 atmosphere. In order to investigate inflammation, the cells (2×10^4 cells/mL) were seeded onto the ZrO_2 specimens, including lipopolysaccharide (LPS) non-treated **ZrO_2-1** (negative control), LPS treated **ZrO_2-1** (positive control),

ZrO_2-2, **3′**, **5** and **7**. These were put into a 40 well culture plate and incubated. After 24 h of culture, the cells were harvested to isolate total RNA. The primers for TNF-α were 5′-GGC AGG TCT ACT TTG GAG TCA TTG C-3′ (sense) and 5′-ACA TTC GAG GCT CCA GTG AAT TCG G-3′ (antisense), the primers for IL-6 were 5′-CTG GTG ACA ACC ACG GCC TTC CCT A-3′ (sense) and 5′-ATG CTT AGG CAT AAC GCA CTA GGT T-3′ (antisense) and the primers for glyceraldehyde 3-phosphate dehydrogenase (GAPDH) were 5′-ACT TTG TCA AGC TCA TTT CC-3′ (sense) and 5′-TGC AGC GAA CTT TAT TGA TG-3′ (antisense). Reverse-transcription polymerase chain reaction (RT-PCR) amplifications on all of the ZrO_2 specimens were carried out for 35 cycles at 94 °C for 30 s, at 55–60 °C for 1 min, and at 72 °C for 1 min after the initial denaturation step at 94 °C for 5 min. The reverse transcriptase-polymerase chain reaction (RT-PCR) products of all of the ZrO_2 specimens were separated on 1% agarose gel and visualized by ethidium bromide.

2.7. MG-63 cell proliferation of *ZrO_2-1, 3′ and 4–7*

MG-63 cells were cultured in DMEM supplemented with 10% of FBS, 1% penicillin-streptomycin, at 37 °C in 5% CO_2. MG-63 cells, suspended in 50 μL of the medium, were loaded onto the upper surfaces of **ZrO_2-1**, **3′** and **4–7** with a micropipette, respectively. After 4 h, all of the ZrO_2 specimens were placed into a fresh and sterile 24 well culture plate and 1 mL of pure medium was added. The plate was cultured in a humidified incubator at 37 °C and 5% of CO_2 for 1, 4, and 7 days. In order to investigate cell morphology, the MG-63 cells were fixed and dehydrated for SEM observation after 7 days of culture. The proliferation of MG-63 cells was evaluated by using a cell counting kit (CCK-8, Dojindo Molecular Technologies Inc., USA) assay.

2.8. ALP activity of *ZrO_2-1, 3′ and 4–7*

The level of ALP, a marker of osteogenic differentiation from MG-63 cells, was measured using a spectroscopic method. The surfaces of **ZrO_2-1**, **3′** and **4–7** were seeded with MG-63 cells at a density of 1×10^5 cell/mL and were cultured for 7 and 14 days. Afterwards these were washed with PBS (pH 7.4) three times, sonicated with 3 mL lysis buffer solution (0.1% Triton X-100, Sigma, St. Louis, MO, USA) using a Vibra Cell™ (Sonics & Materials Inc., Danbury, CT, USA) for 1 min at 110 W (50/60) in ice. Sonicated cell-constructs were then purified by centrifugation at 14,000 rpm at 4 °C for 15 min. Supernatants were collected from the cell-constructs. The enzyme reaction was set up by mixing 6 μL of the supernatants with 54 μL of 0.02% lysis buffer containing 100 μL of 1 M Tris–HCl (Sigma, pH 9.0), 20 μL of 5 mM $MgCl_2$, and 20 μL of 5 mM para-nitrophenyl phosphate (PNPP). The solution was incubated at 37 °C for 30 min and the reaction was then stopped by adding 500 μL of 1 N NaOH solution. The level of *p*-nitrophenol production in the presence of ALPase was measured by monitoring the light absorbance of the solution at 405 nm using a microplate reader. The data were expressed as unit/min/mg protein.

2.9. Calcium deposition of The functionalized-*1, 3′ and 4–7*

After 7, 14, and 21 days of incubation, **ZrO_2-1**, **3′** and **4–7** seeded with MG-63 cells at a density of 1×10^5 cells/mL were rinsed with fresh PBS (pH 7.4) and then fixed with 70% ethanol at −20 °C for 1 h. All of the fixed ZrO_2 specimens were stained with 2% Alizarin red S staining solution (adjusted to pH 4.2 with 10% of ammonium hydroxide) for 20 min, and then rinsed with fresh PBS, respectively. The formation of a nodule was observed by using an optical photograph. In order to quantitatively investigate, all of the rinsed ZrO_2 specimens were desorbed with 10% cetylpyridinium chloride. The deposition of calcium was determined by measuring the absorbance at 540 nm using a microplate reader.

2.10. RT-PCR for ALP, runt-related transcription factor 2 (RUNX2), osteopontin (OP) and osteocalcin (OC) mRNA expressions of *ZrO_2-1, 3′ and 4–7*

The isolations of total RNA in MG-63 cells (2×10^4 cells/mL) cultured on **ZrO_2-1**, **3′** and **4–7** were carried out by using an RNeasy Plus Mini Kit (Qiagen, CA, USA). The total RNA (1 μg) of the cells extracted from all of the ZrO_2 specimens were reversely transcribed into cDNA by using AccuPower RT PreMix (Bioneer, Daejeon, Republic of Korea) according to manufacturer's instructions. RT-PCR amplifications on all of the ZrO_2 specimens were carried out by using an AccuPower PCR PreMix (Bioneer, Daejeon, Republic of Korea). The primers for ALP were 5′-CCG TGG CAA CTC TAT CTT TG-3′ (sense) and 5′-GCC ATA CAG GAT GGC AGT GA-3′ (antisense). The primers for RUNX2 were 5′-CCA ACT TCC TGT GCT CCG TG-3′ (sense) and 5′-TCT TGC CTC GTC CGC TCC-3′ (antisense). The primers for OP were 5′-ACA TCA CCT CAC ACA TGG AAA GC-3′ (sense) and 5′-GCT GAC TCG TTT CAT AAC TGT CCT-3′ (antisense). The primers for OC were 5′-GTC CAA GCA GGA GGG CAG-3′ (sense) and 5′-TTG AGC TCA CAC ACC TCCC C-3′ (antisense). The primers for GAPDH were 5′-ACT TTG TCA AGC TCA TTT CC-3′ (sense) and 5′-TGC AGC GAA CTT TAT TGA TG-3′ (antisense). RT-PCR amplifications on all specimens were carried out for 35 cycles at 94 °C for 30 s, followed by 55–60 °C for 1 min, and then held at 72 °C for 1 min after the initial denaturation step at 94 °C for 5 min. The RT-PCR products of all of the specimens were separated on 1% of agarose gel and visualized by ethidium bromide.

2.11. Statistical analysis

All experiments were carried out in triplicate. One-way analysis of variance (ANOVA) and the Tukey *post hoc* test were used to assess the normally distributed data and the results were reported as mean ± SD. Statistical significance was accepted at $^*p < 0.05$.

3. Results

3.1. Surface characterization of *ZrO_2-1, 2,and 3′*

The surface morphologies of lyophilized **ZrO_2-3′** were characterized by SEM and TM-AFM observations and compared with **ZrO_2-1** and **2**. SEM observations of dried surfaces at magnifications of 300× and 1.0k× showed a series of fibrous strands throughout the **ZrO_2-3′** surface (Fig. 2A(c and d)), whereas the surfaces of **ZrO_2-1** and **2** did not show any remarkable differences (Fig. 2A(a and b)). The TM-AFM images of **ZrO_2-3′** were also observed (Fig. 2B(b)). TM-AFM images observed on wet surfaces displayed swelled fibrous strands, indicating the effect of the adsorbed MES buffer solution. However, the fibrous strands were not completely covered on the **ZrO_2-1** surface. **ZrO_2-2** showed a similar morphology to **ZrO_2-1** (data not shown). It was found that the surface of **ZrO_2-3′** was covered with more fibrous strands than **ZrO_2-1** and **2** (Fig. 2B).

The chemical compositions of **ZrO_2-1**, **2** and **3′** were characterized by wide-scanning XPS measurement (Fig. 2C). It was found that N1s exist on **ZrO_2-2** and **3′** which indicates the existence of APTES. Moreover, it was found that the O1s percentage on **ZrO_2-3′** was the highest (Table 1). This result indicates that HA was conjugated on the surface of **ZrO_2-2** (**ZrO_2-3**). These results correlate with the results of contact angle measurements. Due to hydrophilic HA, the contact angle of **ZrO_2-3′** was the lowest (Table 1).

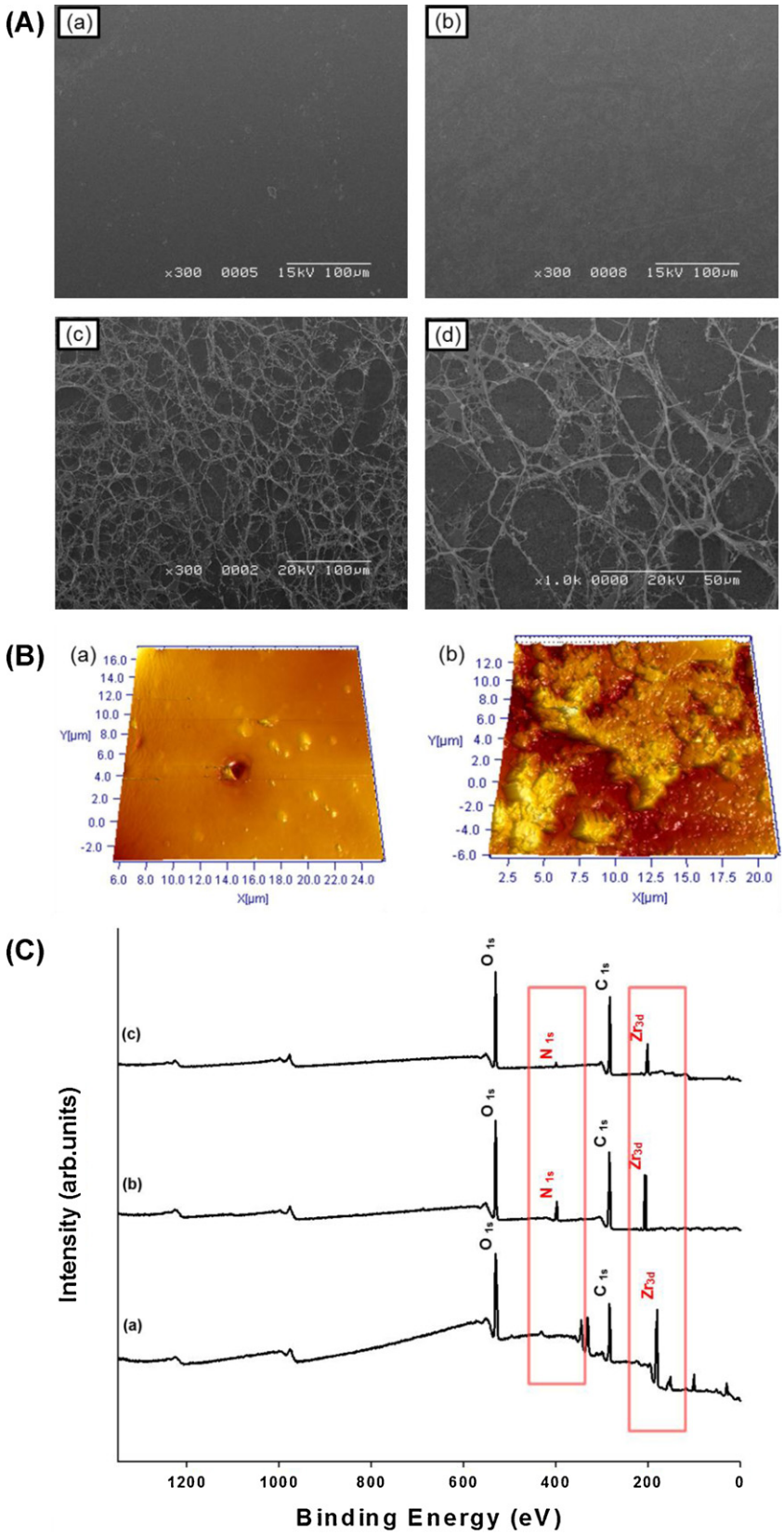

Fig. 2. (A) Surface morphology images of (a) **Zr-1**, (b) **Zr-2** and (c and d) **Zr-3**. **Zr-1** and **2** were observed at a magnification of 300×. **Zr-3** was observed at magnifications of (c) 300× and (d) 1.0k×, respectively. (B) TM-AFM images of (a) **Zr-1** and (b) **Zr-3**. (C) Wide-scanned XPS spectra of (a) **Zr-1**, (b) **Zr-2** and (c) **Zr-3**. The spectra were measured from 0 to 1350 eV.

Table 1
Percentages of O1s, N1s, C1s and Zr3d existing on **Zr-1–3**, and their contact angles.

	O1s (%)	N1s (%)	C1s (%)	Zr3d (%)	Contact angle (°)
Zr-1	31.09	–	27.94	40.97	79.98 ± 0.57
Zr-2	27.88	10.15	26.09	35.88	60.15 ± 0.94
Zr-3	39.44	7.63	23.78	29.15	15.15 ± 0.03

3.2. Protein adsorption of ZrO_2-1, 2 and 3′

The non-specific adsorption behavior of BSA on **ZrO_2-3′** was measured as compared to those of **ZrO_2-1** and **2** (Fig. 3). After 6 and 24 h, significantly higher amounts of albumin was present on **ZrO_2-3′** surface than on the other ZrO_2 specimens. This result was in accordance with the previous report (Huang et al., 2011).

3.3. Release kinetics of BMP-2 and GDF-5 from ZrO_2-4–7

The existing amounts of BMP-2 and GDF-5 in **ZrO_2-4–7** were measured, and their actual loading amounts were approximately 7.42 ± 0.92 ng and 7.1 ± 0.72 ng (**ZrO_2-4** and **6**), 39.7 ± 1.35 and 38.9 ± 2.23 ng (**ZrO_2-5** and **7**), respectively as compared to the initial loading amounts (10 ng/**ZrO_2-4** and **6**, and 50 ng/**ZrO_2-5** and **7**). It was found that the initial bursts of BMP-2 and GDF-5 from **ZrO_2-4–7** took place within 6 h regardless of the loading amounts. The initial bursts were below 13%, 20%, 23%, and 30%, respectively (Fig. 4). The BMP-2 and GDF-5 release from **ZrO_2-4** and **6** reached up to 100% after 28 days, whereas **ZrO_2-5** and **7** were approximately 76% (Fig. 4). These results indicate that the loading amount of BMP-2 and GDF-5 play a significant role in their release kinetics.

3.4. Inflammatory tests of ZrO_2-1, 2 and 3′, 5 and 7

To investigate the degree of biological activation of **ZrO_2-7** compared to **ZrO_2-2**, **3′**, and **5**, RT-PCR was used. For negative and positive controls LPS non-treated and treated **ZrO_2-1** were used, respectively. **ZrO_2-2**, **3′**, **5** and **7** were cultured with RAW 264.7 (mouse macrophage) cells. The results showed that the gene expressions of pro-inflammatory cytokines tumor necrosis factor-alpha (TNF-α) and interleukin-6 (IL-6) mRNA (He, McConnell, Schneider, & Bellamkonda, 2007; Lee et al., 2000; Sowa et al., 2003) were markedly attenuated in **ZrO_2-5** and **7** (Fig. 5). This indicates that **ZrO_2-5** and **7** remain biologically active and possess anti-inflammatory effects. Moreover, it was found that GDF-5 has a significant effect that can inhibit the gene expression of TNF-α and IL-6, similar to BMP-2 (Fig. 5).

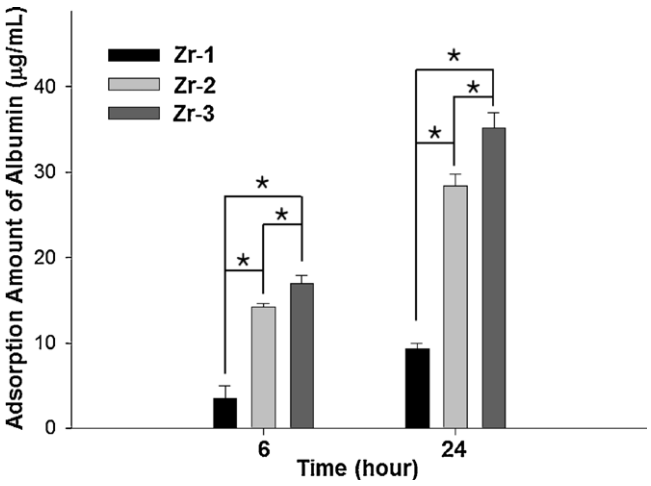

Fig. 3. Amount of BSA adsorbed on the surface of **Zr-1**, **2** and **3** ($n = 3$); $^*p < 0.05$.

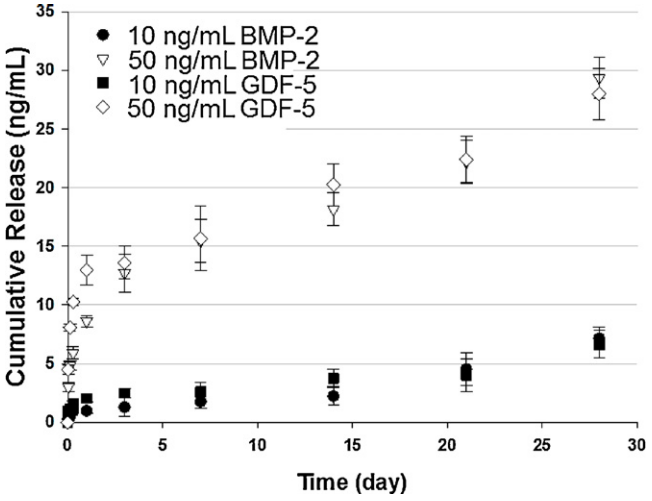

Fig. 4. Release kinetics of GDF-5 and BMP-2 from **Zr-4–7**. The release was measured for 28 days ($n = 3$).

3.5. Proliferation of MG-63 cells on ZrO_2-1, 3′ and 4–7

F-actin staining was carried out to visualize cytoskeletal F-actin fibers which distribute around the membrane. The morphologies and organizations of MG-63 cells seeded on **ZrO_2-1**, **3′** and **4–7** (Fig. 6) were determined as an indication of the proliferation degree of these cells. There were no remarkable differences in the spreading and contact behaviors of the cells on all of the ZrO_2 specimens (Fig. 6A). However, MG-63 cells were observed to show higher attachment to **ZrO_2-5** and 7 after 7 days as compared to **ZrO_2-1**, **3′**, **4** and **6** (Fig. 6B). This result indicates that GDF-5 has a positive influence on the proliferation of MG-63 cells, similar to the effect of BMP-2.

3.6. Differentiation of ZrO_2-1, 3′ and 4–7

Fig. 7A shows ALP activity levels of MG-63 cells cultured on **ZrO_2-1**, **3′** and **4–7** on day 7 and 14. The ALP activity levels of the ZrO_2 specimens were less prevalent after 14 days of culture than after 7 days. There were no significant differences among **ZrO_2-1**, **3′**, **4** and **6**, whereas **ZrO_2-5** and **7** showed significantly higher ALP activity levels at 14 days. These results show that the delivery of BMP-2 and GDF-5 to these cells has a significant influence on accelerating the ALP activity levels. Moreover, it was found that GDF-5 plays a significant role in the acceleration of ALP activity levels, similar to the effect of BMP-2.

Fig. 7B shows the degree of calcium deposition from MG-63 cells cultured on **ZrO_2-1**, **3′** and **4–7** at time points of 7, 14 and 21 days, respectively. It was found that the calcium depositions on all of the ZrO_2 specimens were consistent with results of the ALP activity levels. At 21 days, the calcium depositions of **ZrO_2-5** and **7** were

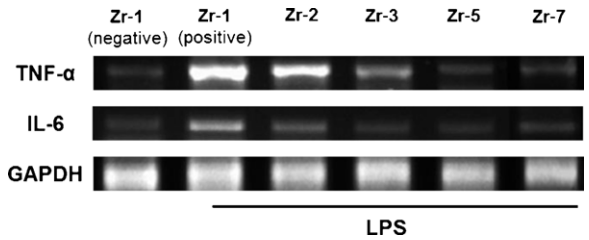

Fig. 5. Evaluation of biological activation of **Zr-7** through inflammatory test as compared to negative and positive controls, and **Zr-2**, **3**, and **5**. LPS non-treated and treated **Zr-1** were used as negative and positive controls, respectively.

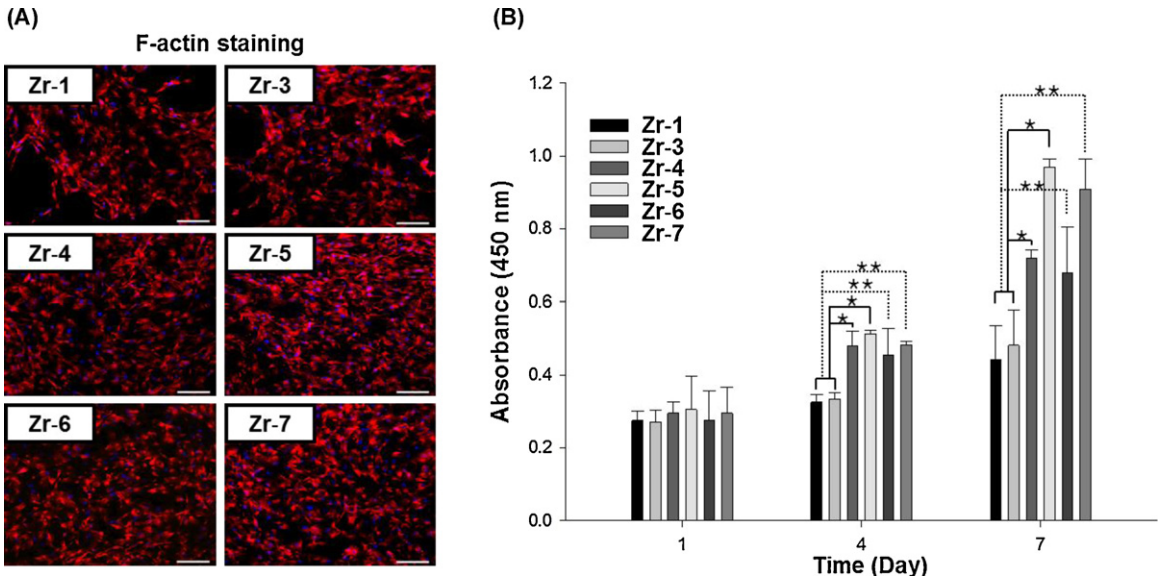

Fig. 6. (A) Visualization of cytoskeletal F-actin fibers as well as the morphology and organization of MG63 cells, and (B) the cell proliferation ($n = 3$); $^{*}p < 0.05$.

higher than those of **ZrO_2-1**, **3′**, **4** and **6**. **ZrO_2-5** showed slightly higher calcium deposition than **ZrO_2-7** (Fig. 7B(a)). At day 21, the extent of mineralized area was in agreement with the results of Fig. 7B(a and b)). These results indicate that GDF-5 has a positive influence on accelerating calcium deposition in a manner similar to the effects of BMP-2.

Fig. 7C shows the mRNA expressions of RUNX2, ALP, OP, and OC of MG-63 cells cultured on **ZrO_2-1**, **3′** and **4–7**, respectively. The results were normalized to GAPDH expression. RUNX2 is a transcription factor associated with osteoblastic differentiation and regulates the expression of osteo-specific genes including ALP, OP, and OC (Sowa et al., 2003). **ZrO_2-5** and **7** showed higher mRNA expressions of ALP, OP, and OC than **ZrO_2-1**, **3′**, **4** and **6** for up to 28 days even though the expression of RUNX-2 was marginal among **ZrO_2-4–7**. The mRNA expressions were higher when the loading amounts of BMP-2 and GDF-5 were elevated, respectively. From

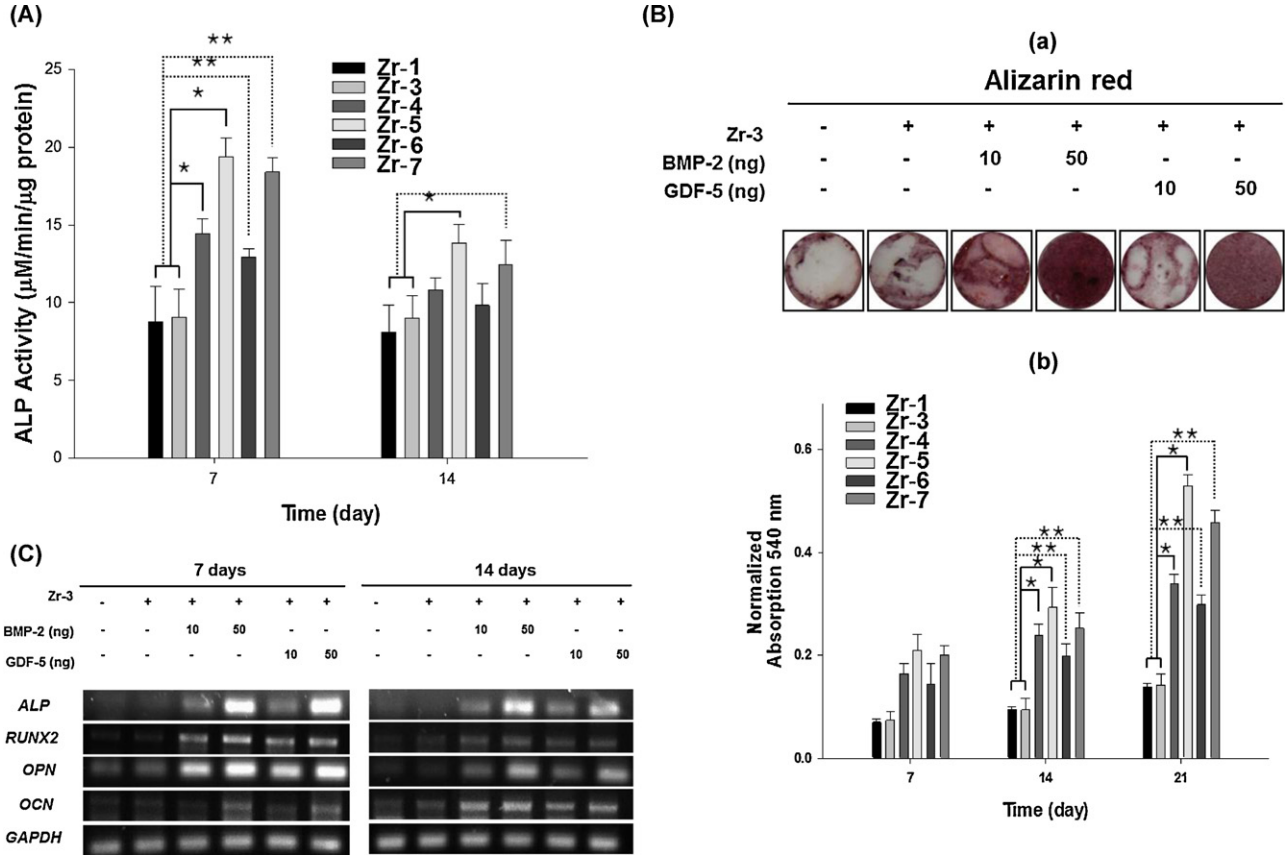

Fig. 7. (A) ALP activity levels of MG-63 cells cultured on **Zr-1**, **3–7** at the time points of 7 and 14 days. (B) Deposition degree of calcium from MG-63 cells cultured on **Zr-1**, **3–7**. (C) mRNA expression of RUNX2, ALP, OPN, and OCN of MG-63 cells cultured on **Zr-1**, **3–7**. This experiments were carried out in triplicate; $^{*}p < 0.05$.

these results, it is shown that the loading of BMP-2 and GDF-5 into the hydrogels has a significant influence on osteoblastic differentiation. Moreover, it was found that GDF-5 was positively influential on accelerating new bone formation, similar to BMP-2.

4. Discussion

The results presented in this study showed that functionalized **ZrO_2-4–7** containing GDF-5 as well as BMP-2 can potentially aid in improving osteoblastic differentiation. This could be of great significance for long-term implantation of biomedical devices in the human body. It is well known that biocompatibility and biological function are the most important factors for dental implant materials (Matsuno, Yokoyama, Watari, Uo, & Kawasaki, 2001). To this end, it is necessary to improve the biocompatibility and biological function using physical and chemical modifications.

The BSA adsorption test showed that protein adsorption was relatively higher on **ZrO_2-3′** as compared to **ZrO_2-1** and **2**, suggesting that BSA is adsorbed into the swollen HA gel existing on **ZrO_2-3′**. Generally, the adsorption of albumin has a significant influence on the proliferation and differentiation of MG-63 cells (Huang et al., 2011). These results can possibly be related to the higher MG-63 cell proliferation and differentiation observed on the protein adsorbing **ZrO_2-3′** as compared to **ZrO_2-1** and **2** (Fig. 3).

Osteogenic differentiation factors, BMP-2 and GDF-5, have been reported to increase the proliferation and differentiation of pre-osteoblastic cells (Schwarz et al., 2009). However, the research on GDF-5 is relatively rare as compared to BMP-2. Also, it has been known that transforming growth factor beta (TGF-β) superfamily improves bone anabolic effects in both *in vitro* and *in vivo* conditions (Karsdal, Martin, Bollerslev, Christiansen, & Henriksen, 2007). To create an effective delivery system that can release the osteogenic differentiation factors with appropriate release time and amount. The initial bursts of **ZrO_2-4–7** in the 6 h were 13%, 20%, 23%, and 30%, respectively. Over a period of 28 days, 96%, 74%, 94%, and 71% of BMP-2 and GDF-5 released from the **ZrO_2-4–7**, respectively. In this system, we found that BMP-2 and GDF-5 were loaded into **ZrO_2-3′** and could be released from **ZrO_2-3′** in a sustained manner with reduced initial burst (Fig. 4).

LPS endotoxins have been known to elicit strong immune responses *in vitro* and induces TNF-α expression *in vitro* and *in vivo* (Covert, Leung, Gaston, & Baltimore, 2005; Lee et al., 2000). The expression of GAPDH gene was used as a control for the values for TNF-α and IL-6 mRNA expressions. TNF-α and IL-6 play important mediator roles in immune processes (He et al., 2007). Several cellular *in vitro* tests such as anti-inflammatory tests using RAW264.7 cells, proliferation tests using MG-63 cells, ALP activity tests, and mineralization tests were used to confirm the cytocompatibility of the material.

There is a general agreement that only these mature osteoblasts have the potential to synthesize and assemble relevant bone matrix for osseointegration. Osseointegration is one of the important key steps for dental implants in dentistry. Osteogenic markers (ALP, OP, OC) have the potential to synthesize and assemble relevant bone matrix for osseointegration. These observations resulted in distinct osteogenic markers like alkaline phosphatase (ALP), osteopontin (OP), osteocalcin (OC). RT-PCR tests for mRNA expressions of RUNX2, ALP, OP, and OC using MG-63 cells were done and found that **ZrO_2-7** showed a similar capability of new bone formation as compared to **ZrO_2-5**. From this study, we confirmed that the **ZrO_2-3′** has the capability to effectively contain and release osteogenic differentiation factors and therefore can potentially be a candidate for a biomaterial for biomolecules and osteogenic drug delivery. Moreover, the cost effective GDF-5 can be a competitive alternative to BMP-2.

5. Conclusions

We prepared four functionalized ZrO_2 disks, including **ZrO_2-4–7**, and evaluated the feasibility of new bone formation on each disk. The existence of **pcHAgel** on the ZrO_2 surface was confirmed by SEM, AFM and XPS measurements. Albumin, which influences the proliferation and differentiation of MG-63 cells, was well adsorbed on the **ZrO_2-3′**. By an inflammatory response test it was found that GDF-5, similar to BMP-2, can act as an anti-inflammatory factor. The release tests of GDF-5 and BMP-2 showed that the initial burst could be retained below 30% and the two osteogenic differentiation factors are released in a controlled manner for up to 28 days. Through F-actin staining, it was found that MG-63 cells were well proliferated on **ZrO_2-5** and **7**. We found that the existence and loading amount of GDF-5 and BMP-2 have significant influences on ALP activity level, calcium deposition and osteoblastic differentiation. From these results, we suggest that surface-functionalized **ZrO_2-5** and **7** can be used as an implant material for dental applications. Moreover, we suggest that GDF-5 can be useful as an effective osteogenic differentiation factor for accelerating new bone formation.

Acknowledgments

This work was supported by Grant No. 20110007746 from the Basic Research Program of the Korea Science & Engineering Foundation, Grant No. 20110001689 from the Pioneer Research Center Program and Grant No. 20110028336 from Happy Tech. Program through the National Research Foundation of Korea funded by the Ministry of Education.

References

Att, W., Takeuchi, M., Suzuki, T., Kubo, K., Anpo, M., & Ogawa, T. (2009). Enhanced osteoblast function on ultraviolet light-treated zirconia. *Biomaterials*, *30*, 1273–1280.

Bae, M. S., Yang, D. H., Lee, J. B., Heo, D. N., Kwon, Y. D., Yoon, I. C., et al. (2011). Photo-cured hyaluronic acid-based hydrogels containing simvastatin as a bone tissue regeneration scaffold. *Biomaterials*, *32*, 8161–8171.

Brånemark, R., Brånemark, P. I., Rydevik, B., & Myers, R. R. (2001). Osseointegration in skeletal reconstruction and rehabilitation: A review. *Journal of Rehabilitation Research and Development*, *38*, 175–181.

Brunet, L. J., McMahon, J. A., McMahon, A. P., & Harland, R. M. (1998). Noggin, cartilage morphogenesis, and joint formation in the mammalian skeleton. *Science*, *280*, 1455–1457.

Buxton, P., Edwards, C., Archer, C. W., & Francis-West, P. (2001). Growth/differentiation factor-5 (GDF-5) and skeletal development. *The Journal of Bone and Joint Surgery American*, *83-A*(Suppl. 1), S23–S30.

Chevalier, J. (2006). What future for zirconia as a biomaterial? *Biomaterials*, *27*, 535–543.

Choi, J., Konno, T., Matsuno, R., Takai, M., & Ishihara, K. (2008). Surface immobilization of biocompatible phospholipid polymer multilayered hydrogel on titanium alloy. *Colloids and Surfaces B: Biointerfaces*, *67*, 216–223.

Clapper, J. D., Sievens-Figueroa, L., & Guymon, C. A. (2008). Photopolymerization in polymer templating. *Chemistry of Materials*, *20*, 768–781.

Covert, M. W., Leung, T. H., Gaston, J. E., & Baltimore, D. (2005). Achieving stability of lipopolysaccharide-induced NF-kappaB activation. *Science*, *309*, 1854–1857.

Garvie, R. C., Hannink, R. H., & Pascoe, R. T. (1975). Ceramic steel? *Nature*, *258*, 703–704.

Gerecht, S., Burdick, J. A., Ferreira, L. S., Townsend, S. A., Langer, R., & Vunjak-Novakovic, G. (2007). Hyaluronic acid hydrogel for controlled self-renewal and differentiation of human embryonic stem cells. *Proceedings of the National Academy Sciences of the United States of America*, *104*, 11298–11303.

Gruber, R. M., Ludwig, A., Merten, H. A., Pippig, S., Kramer, F. J., & Schliephake, H. (2009). Sinus floor augmentation with recombinant human growth and differentiation factor-5 (rhGDF-5): A pilot study in the Goettingen miniature pig comparing autogenous bone and rhGDF-5. *Clinical Oral Implants Research*, *20*, 175–182.

He, W., McConnell, G. C., Schneider, T. M., & Bellamkonda, R. V. (2007). A novel anti-inflammatory surface for neural electrodes. *Advanced Materials*, *19*, 3529–3533.

Hiemstra, C., Zhou, W., Zhong, Z., Wouters, M., & Feijen, J. (2007). Rapidly in situ forming biodegradable robust hydrogels by combining stereocomplexation and photopolymerization. *Journal of the American Chemical Society*, *129*, 9918–9926.

Hötten, G. C., Matsumoto, T., Kimura, M., Bechtold, R. F., Kron, R., Ohara, T., et al. (1996). Recombinant human growth/differentiation factor 5 stimulates

mesenchyme aggregation and chondrogenesis responsible for the skeletal development of limbs. *Growth Factors*, *13*, 65–74.
Huang, H. M., Hsieh, S. C., Teng, N. C., Feng, S. W., Ou, K. L., & Chang, W. J. (2011). Biological surface modification of titanium surfaces using glow discharge plasma. *Medical & Biological Engineering & Computing*, *49*, 701–706.
Hutchison, J. B., Stark, P. F., Hawker, C. J., & Anseth, K. S. (2005). Polymerizable living free radical initiators as a platform to synthesize functional networks. *Chemistry of Materials*, *17*, 4789–4797.
Jeon, O., Bouhadir, K. H., Mansour, J. M., & Alsberg, E. (2009). Photocrosslinked alginate hydrogels with tunable biodegradation rates and mechanical properties. *Biomaterials*, *30*, 2724–2734.
Karsdal, M. A., Martin, T. J., Bollerslev, J., Christiansen, C., & Henriksen, K. (2007). Are nonresorbing osteoclasts sources of bone anabolic activity? *Journal of Bone and Mineral Research*, *22*, 487–494.
Kim, S. E., Song, S. H., Yun, Y. P., Choi, B. J., Kwon, I. K., Bae, M. S., et al. (2011). The effect of immobilization of heparin and bone morphogenic protein-2 (BMP-2) to titanium surfaces on inflammation and osteoblast function. *Biomaterials*, *32*, 366–373.
Koch, F. P., Becker, J., Terheyden, H., Capsius, B., & Wagner, W. (2010). A prospective, randomized pilot study on the safety and efficacy of recombinant human growth and differentiation factor-5 coated onto beta-tricalcium phosphate for sinus lift augmentation. *Clinical Oral Implants Research*, *21*, 1301–1308.
Kogan, G., Soltés, L., Stern, R., & Gemeiner, P. (2007). Hyaluronic acid: A natural biopolymer with a broad range of biomedical and industrial applications. *Biotechnology Letters*, *29*, 17–25.
Lee, E. G., Boone, D. L., Chai, S., Libby, S. L., Chien, M., Lodolce, J. P., et al. (2000). Failure to regulate TNF-induced NF-kappaB and cell death responses in A20-deficient mice. *Science*, *289*, 2350–2354.
Lee, J. S., Wikesjö, U. M., Jung, U. W., Choi, S. H., Pippig, S., Siedler, M., et al. (2010). Periodontal wound healing/regeneration following implantation of recombinant human growth/differentiation factor-5 in a beta-tricalcium phosphate carrier into one-wall intrabony defects in dogs. *Journal of Clinical Periodontology*, *37*, 271–389.
Matsuno, H., Yokoyama, A., Watari, F., Uo, M., & Kawasaki, T. (2001). Biocompatibility and osteogenesis of refractory metal implants, titanium, hafnium, niobium, tantalum and rhenium. *Biomaterials*, *22*, 1253–1262.
Morotome, Y., Goseki-Sone, M., Ishikawa, I., & Oida, S. (1998). Gene expression of growth and differentiation factors-5, -6, and -7 in developing bovine tooth at the root forming stage. *Biochemical and Biophysical Research Communications*, *244*, 85–90.
Piconi, C., Burger, W., Richter, H. G., Cittadini, A., Maccauro, G., Covacci, V., et al. (1998). Y-TZP ceramics for artificial joint replacements. *Biomaterials*, *19*, 1489–1494.
Pourbaix, M. (1984). Electrochemical corrosion of metallic biomaterials. *Biomaterials*, *5*, 122–134.
Schwarz, F., Ferrari, D., Sager, M., Gerten, M., Gartig, B., & Becker, J. (2009). Guided bone regeneration using rhGDF-5 and rhBMP-2-coated natural bone mineral in rat calvarial defects. *Clinical Oral Implants Research*, *20*, 1219–1230.
Sena, K., Morotome, Y., Baba, O., Terashima, T., Takano, Y., & Ishikawa, I. (2003). Gene expression of growth differentiation factors in the developing periodontium of rat molars. *Journal of Dental Research*, *82*, 166–171.
Sidorenko, A., Krupenkin, T., Taylor, A., Fratzl, P., & Aizenberg, J. (2007). Reversible switching of hydrogel-actuated nanostructures into complex micropatterns. *Science*, *315*, 487–490.
Sowa, H., Kaji, H., Canaff, L., Hendy, G. N., Tsukamoto, T., Yamaguchi, T., et al. (2003). Inactivation of menin, the product of the multiple endocrine neoplasia type 1 gene, inhibits the commitment of multipotential mesenchymal stem cells into the osteoblast lineage. *Journal of Biological Chemistry*, *278*, 21058–21069.
Tokarev, I., & Minko, S. (2010). Stimuli-responsive porous hydrogels at interfaces for molecular filtration, separation, controlled release, and gating in capsules and membranes. *Advanced Materials*, *22*, 3446–3462.
Uchida, M., Kim, H. M., Miyaji, F., Kokubo, T., & Nakamura, T. (2002). Apatite formation on zirconium metal treated with aqueous NaOH. *Biomaterials*, *23*, 313–317.
Webster, T. J., Ergun, C., Doremus, R. H., Siegel, R. W., & Bizios, R. (2000). Enhanced functions of osteoblasts on nanophase ceramics. *Biomaterials*, *21*, 1803–1810.
Yakushiji, T., Sakai, K., Kikuchi, A., Aoyagi, T., Sakurai, Y., & Okano, T. (1999). Effects of cross-linked structure on temperature-responsive hydrophobic interaction of poly(N-isopropyl-acrylamide) hydrogel-modified surfaces with steroids. *Analytical Chemistry*, *71*, 1125–1130.